



The POKEMON Speckle Survey of Nearby M Dwarfs. I. New Discoveries

Catherine A. Clark^{1,2}, Gerard T. van Belle², Elliott P. Horch³, Kaspar von Braun², David R. Ciardi⁴,
Jennifer G. Winters⁵, and Rocío Kiman⁶

¹Northern Arizona University, 527 South Beaver Street, Flagstaff, AZ 86011, USA; catclark@nau.edu

²Lowell Observatory, 1400 West Mars Hill Road, Flagstaff, AZ 86001, USA

³Southern Connecticut State University, 501 Crescent Street, New Haven, CT 06515, USA

⁴NASA Exoplanet Science Institute Caltech/IPAC, Pasadena, CA 91125, USA

⁵Center for Astrophysics | Harvard & Smithsonian, 60 Garden Street, Cambridge, MA 02138, USA

⁶Kavli Institute for Theoretical Physics, University of California, Santa Barbara, CA 93106, USA

Received 2022 April 7; revised 2022 May 23; accepted 2022 May 24; published 2022 July 4

Abstract

M dwarfs are favorable targets for exoplanet detection with current instrumentation, but stellar companions can induce false positives and inhibit planet characterization. Knowledge of stellar companions is also critical to our understanding of how binary stars form and evolve. We have therefore conducted a survey of stellar companions around nearby M dwarfs, and here we present our new discoveries. Using the Differential Speckle Survey Instrument at the 4.3 m Lowell Discovery Telescope, and the similar NN-EXPLORE Exoplanet Stellar Speckle Imager at the 3.5 m WIYN telescope, we carried out a volume-limited survey of M-dwarf multiplicity to 15 parsecs, with a special emphasis on including the later M dwarfs that were overlooked in previous surveys. Additional brighter targets at larger distances were included for a total sample size of 1070 M dwarfs. Observations of these 1070 targets revealed 26 new companions; 22 of these systems were previously thought to be single. If all new discoveries are confirmed, then the number of known multiples in the sample will increase by 7.6%. Using our observed properties, as well as the parallaxes and 2MASS K magnitudes for these objects, we calculate the projected separation, and estimate the mass ratio and component spectral types, for these systems. We report the discovery of a new M-dwarf companion to the white dwarf Wolf 672 A, which hosts a known M-dwarf companion as well, making the system trinary. We also examine the possibility that the new companion to 2MASS J13092185-2330350 is a brown dwarf. Finally, we discuss initial insights from the POKEMON survey.

Unified Astronomy Thesaurus concepts: [Binary stars \(154\)](#); [Visual binary stars \(1777\)](#); [Low mass stars \(2050\)](#); [High angular resolution \(2167\)](#); [Speckle interferometry \(1552\)](#); [Close binary stars \(254\)](#); [M dwarf stars \(982\)](#); [White dwarf stars \(1799\)](#)

1. Introduction

Though they are the smallest and least luminous stars on the main sequence, the M dwarfs occupy a captivating range of stellar parameter space. Their masses span nearly a factor of ten (Baraffe & Chabrier 1996), and the lowest-mass M dwarfs have main-sequence lifetimes of trillions of years (Laughlin et al. 1997). Additionally, the M dwarfs dominate the galactic neighborhood, accounting for approximately 75% of the stars in the Milky Way (Henry et al. 2006). The M dwarfs also offer a significant opportunity for finding and characterizing Earth-sized planets (e.g., López-Morales et al. 2019), due to their relatively small star-to-planet mass and radius ratios, as well as their sheer numbers.

However, one property that can inhibit the detection and characterization of the planets that orbit M dwarfs is stellar multiplicity. “Third light” contamination of light curves, which is caused by stellar companions, has been shown to inhibit the detection of Earth-sized, transiting planets (Lester et al. 2021), and has led to additional obstacles in planet characterization including underestimated planet radii (Ciardi et al. 2015), skewed planet radius distributions and occurrence rates (Hirsch et al. 2017; Bouma et al. 2018; Teske et al. 2018), incorrect

characterization of both stars’ properties (Furlan & Howell 2020), and improper mean density and atmospheric values (Howell 2020). Additionally, close-in stellar companions can perturb and truncate protoplanetary disks (Jang-Condell 2015), gravitationally excite planetesimals causing collisional destruction (Rafikov & Silsbee 2015a, 2015b), and scatter and eject planets that have formed (Haghighipour & Raymond 2007). Furthermore, recent studies have suggested that even wide stellar companions might affect the formation or orbital properties of giant planets (e.g., Fontanive et al. 2019; Fontanive & Bardalez Gagliuffi 2021; Hirsch et al. 2021; Su et al. 2021; Mustill et al. 2022). As the M dwarfs have proven to be such favorable targets for planet detection and characterization, measuring their multiplicity is therefore crucial to understanding the planets that they host.

Furthermore, work on Kepler (Borucki et al. 2011), K2 (Howell et al. 2014), and now TESS (Ricker et al. 2015) suggests that the stellar companions to exoplanet hosts have longer orbital periods than the companions to field stars (e.g., Kraus et al. 2012; Bergfors et al. 2013; Wang et al. 2014; Kraus et al. 2016; Ziegler et al. 2020; Hirsch et al. 2021; Howell et al. 2021; Lester et al. 2021; Moe & Kratter 2021; Clark et al. 2022). Multiplicity measurements are therefore critical to understanding M-dwarf system architectures and occurrence rates as well.

Because of the significance M dwarfs have for both stellar astrophysics and exoplanet studies, many surveys have been carried out to determine the M-dwarf multiplicity rate,

especially in recent years. It has been shown that multiplicity decreases with mass from O to M (e.g., Mason et al. 2009; Raghavan et al. 2010; Duchêne & Kraus 2013; Winters et al. 2019), but this multiplicity has not been fully characterized for M dwarfs, particularly for the later subtypes, due to their faintness and to resolution limits. This is highlighted by the fact that a reasonably complete inventory of later M dwarfs did not exist until recently (e.g., Kirkpatrick et al. 2014; Luhman & Sheppard 2014; Winters et al. 2021). Winters et al. (2019) produced the most comprehensive M-dwarf multiplicity study to date: an all-sky, volume-limited survey that extends to 25 pc. However, their study surveyed binaries with separations larger than $2''$. The study presented here therefore complements the Winters et al. (2019) survey by exploring the inner regions around nearby M dwarfs with high-resolution imaging.

Here we present the 26 new discoveries detected throughout the Pervasive Overview of “Kompanions” of Every M dwarf in Our Neighborhood (POKEMON) survey, which identified companions to nearby M dwarfs at large-telescope, diffraction-limited resolution. The POKEMON survey is volume-limited through M9, out to at least 15 pc, with additional brighter targets at larger distances, resulting in a sample of 1070 nearby M dwarfs. A future paper will present the full sample of M dwarfs we surveyed, the completeness of the survey, and our updated M-dwarf multiplicity rate. Additionally, though Janson et al. (2012) calculated M-dwarf multiplicity by spectral subtype through M6, our upcoming paper will establish the M-dwarf multiplicity rate by subtype through M9 for the first time. This initial paper in the series presents and characterizes the new discoveries that have been revealed by the POKEMON survey.

In Section 2, we describe our target selection process, observational routine, and data reduction procedure. In Section 3, we note systems with both a new discovery and a known companion, and we provide observed properties for the systems with new discoveries. We also assess the likelihood that these new discoveries are bound. Additionally, we estimate astrophysical properties for the systems with new discoveries using the observed properties and parallaxes from the literature. In Section 4, we discuss a system with both a known M dwarf and a known white dwarf, a system with a potential brown dwarf companion, and initial insights from the POKEMON survey. We summarize our conclusions and discuss future work in Section 5.

2. Observations

The POKEMON survey used speckle interferometry (Labeyrie 1970), also known as speckle imaging, to observe 1070 M dwarfs throughout the northern sky.

2.1. Target Selection

The initial basis for our target selection was the seminal Catalog of Nearby Stars (CNS3; Gliese & Jahreiß, 1991), with updates from recent nearby neighbor discoveries from surveys such as RECONS (Henry et al. 2006; Winters et al. 2015) and 2MASS (Skrutskie et al. 2006). A preliminary review of these augmented CNS3 data indicated 522 objects out to 15 pc either identified specifically as M dwarfs, or as potential M dwarfs from $H - K$ color and absolute magnitude M_V . Out to 25 pc, this review resulted in approximately 1500 objects.

We expanded this list to include the ALLWISE Motion Survey (Kirkpatrick et al. 2014) with 3525 new high proper motion objects, and the similar (but nonoverlapping) study by Luhman & Sheppard (2014) that identified 762 high proper motion objects. An examination of the formers new high proper motion objects, using the spectral type-color relationships from Luhman & Sheppard (2014), indicated that there were ~ 350 additional objects between the spectral types of M4 and M9. Other surveys that were mined included the Database of Ultracool Parallaxes based on the Hawaii Infrared Parallax Program (Dupuy & Liu 2012), the CARMENES and APOGEE input catalogs (Deshpande et al. 2013; Alonso-Floriano et al. 2015), and the 2016 release of the Pan-STARRS Parallax and Proper Motion Catalog (Waters et al. 2015), which already had a specific focus on identifying nearby low-mass stars (Magnier et al. 2015).

Given our use of northern hemisphere facilities, a decl. cut of $\delta > -30^\circ$ was carried out. A cut at 15.5 in the I band was also necessary for most objects due to the faint limit of the instruments. These cuts resulted in a sample consisting of 1070 objects.

We note that the parallax sources we used to create the original sample were not perfect; newer astrometric data from Gaia (Gaia Collaboration 2018, 2021) have now provided us with more accurate and precise parallax measurements that indicate some stars in our sample are at distances larger than 15 pc. We chose to keep these stars in the sample despite being farther than previously thought. Parallaxes for these objects are discussed further in Section 3.3.

We present our sample in Figure 1, which is an Aitoff projection showing sky locations of the single and multiple stars in the full sample, compared with the sky locations of the 26 new companions.

2.2. Observational Routine

We imaged the 1070 M dwarfs in the POKEMON sample over 50 nights between UT 2017 April 7 and UT 2020 February 10. The main instrument used in the survey was the Differential Speckle Survey Instrument (DSSI; Horch et al. 2009), which was resident at the 4.3 m Lowell Discovery Telescope (LDT) in Happy Jack, AZ, throughout the POKEMON survey. For brighter targets ($V < 11$), we used the NN-EXPLORE Exoplanet Stellar Speckle Imager (NESSI; Scott et al. 2018), which was used on the 3.5 m WIYN telescope at Kitt Peak National Observatory outside Tucson, AZ.

DSSI and NESSI produce diffraction-limited images from speckle patterns observed simultaneously at two wavelengths. Each instrument uses a dichroic filter to split the collimated beam from the telescope at ~ 700 nm into two channels that are imaged on separate high-speed readout EMCCDs. The standard filter arrangement is 692 and 880 nanometers (nm) for DSSI, and 562 and 832 nm for NESSI, each with 40, 44, or 50 nm bandpasses. The limiting spatial resolution of these instruments at the telescopes we used is ~ 40 milliarcseconds (mas), which is comparable to the near-infrared adaptive optics observing on the Keck II Telescope. These speckle cameras can therefore identify stellar companions down to the ~ 1 au scale.

Bright objects ($V < 11$) require only ~ 1 – 2 minutes of observing time, during which the speckle camera obtains a single image cube of 1000 40 ms speckle frames; these short exposures are necessary to “freeze” out the atmosphere in our

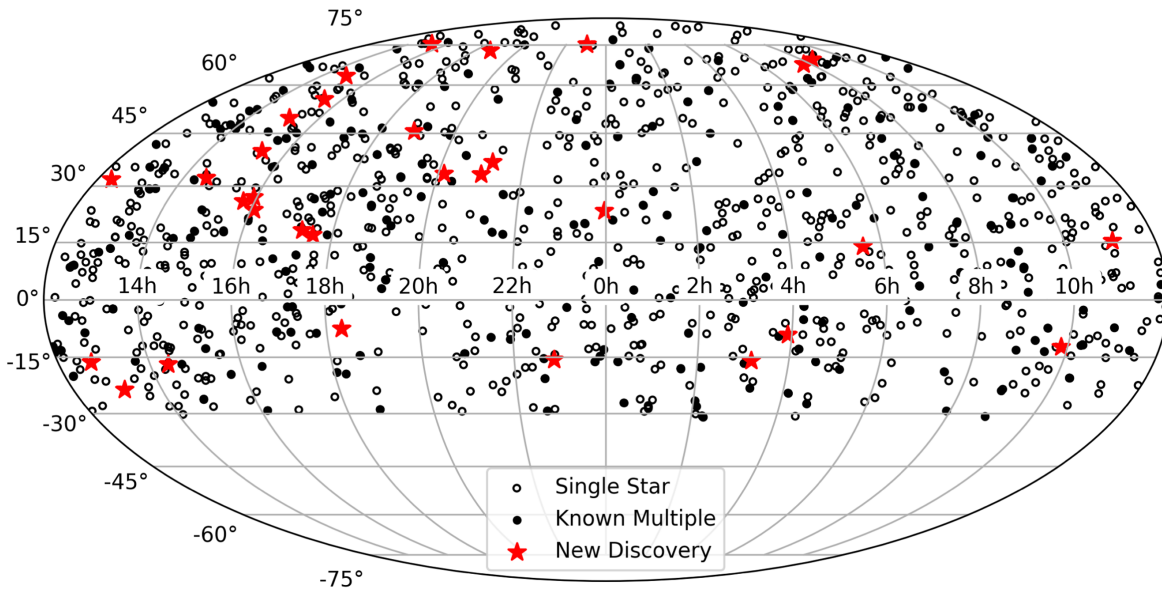


Figure 1. The sky locations of the 1070 stars in the POKEMON sample. 290 of these are known multiples. Single stars are marked with open black circles, known multiples are marked with filled black circles, and the 26 systems with new discoveries are marked with larger, red stars.

observations and to obtain good speckle contrast. Fainter stars ($11 < V < 15.5$) require up to ~ 10 minutes of observing time per target, during which the speckle camera obtains up to nine image cubes. Standard observing also includes periodic observations of bright, unresolved, single stars from the Bright Star Catalog (Hoffleit & Jaschek 1982) to probe the atmospheric conditions experienced by the target of interest. All data cubes are stored as multiextension FITS files.

The pixel scale and image orientation are empirically confirmed by observing binaries with extremely well-known orbits (those listed as Grade 1 in the Sixth Orbit Catalog; Hartkopf et al. 2001). Their ephemeris positions are computed based on the orbital elements, and their scale and orientation are derived from these results. We assume that the calibrations from Horch et al. (2021) are also appropriate for this work, given that our targets were observed on the same runs, besides those observed in February 2020. Figure 3 of Horch et al. (2021) shows the derived uncertainties from the known orbital elements that we have incorporated into our analysis. However, Horch et al. (2021) did not include data from 2020 February. To reduce and analyze this data, we used pixel scale values that were approximate, and that may be updated in the future; the position angle and angular separation values from this run may therefore be updated in the future as well.

It should be noted during our first observing run, from UT 2017 April 7 to UT 2017 April 17, the narrowband speckle filters were not installed within DSSI. When observing without filters, more light reaches the detector, but there is less contrast in the speckles. Furthermore, when filters are not used, significant chromatic effects arise at higher airmasses. We did find that the majority of our newly detected companions were first, or only, detected during this observing run. However, we returned to using the speckle filters for all other observing runs in order to increase the contrast in the speckles. Nonetheless, we plan to investigate the possibility of observing without speckle filters further in the future, both to confirm companions observed only during a single epoch, and to probe new speckle imaging discovery space. The most unique discovery from our filterless observations is discussed further in Section 4.2.

Our observations of the new companions are summarized in Table 1. The 2MASS ID, common name or identifier (if applicable), UT date, telescope, bandpass (λ), and bandpass width ($\Delta\lambda$) are listed. For the filterless observations, instead of listing the bandpass and bandpass width of the observation, we instead indicate whether the companion was detected in the “blue” ($\lambda \lesssim 700$ nm) image or the “red” ($\lambda \gtrsim 700$ nm) image. We note that many of the new discoveries were only detected in the “red” image, since the M dwarfs emit most strongly at near-infrared wavelengths.

2.3. Data Reduction

The data are reduced with a version of the bispectrum speckle reduction code described in Horch et al. (2009, 2011a, 2011b), which uses bispectral analysis (Lohmann et al. 1983) to compute a reconstructed image. This code uses the fact that binary systems produce a fringe pattern in the Fourier plane. A 2D autocorrelation function is calculated for each speckle frame and summed over all frames. The Fourier transform of the autocorrelation function is found and squared to obtain the power spectrum, which is normalized. After dividing by the power spectrum of a point source, the residual 2D power spectrum appears as a set of fringes for each pair of stars in the field. This is fit using a cosine-squared function to determine the relative astrometry and photometry (position angle, angular separation, and delta magnitude) of any pairs of stars in the field. Reconstructed images are constructed from the object’s modulus (the square root of the power spectrum), and the phase estimate is obtained from the bispectrum.

By examining annuli in the reconstructed image that are centered on the primary star, we determine all local maxima and minima in the annulus, and derive their mean value and standard deviation. We then estimate the detection limit as the mean value of the maxima plus five times the average sigma of the maxima and minima. In doing so, the data reduction pipeline produces a curve of this detection limit as a function of separation. Example data demonstrating the reconstructed image and contrast curve are shown in Figure 2.

Table 1
Summary of Observations for Targets with a New Companion

2MASS ID	Name	UT Date (YYYY-MM-DD)	Telescope	λ (nm)	$\Delta\lambda$ (nm)
03104962 – 1549408	LP 772-11	2017-10-20	LDT	880	50
03542561 – 0909316		2017-10-21	LDT	880	50
07011725 + 1348085	G 110-29	2017-4-15	LDT	red	...
07411976 + 6718444	LP 58-260	2017-4-17	LDT	red	...
09510964 – 1219478	GJ 369	2017-5-7	LDT	880	50
11030845 + 1517518	L 1258-55	2017-4-17	LDT	blue	...
...	...	2017-4-17	LDT	red	...
...	...	2018-1-31	LDT	692	40
...	...	2018-1-31	LDT	880	50
12190600 + 3150433	LTT 13435	2017-4-17	LDT	blue	...
...	...	2017-4-17	LDT	red	...
...	...	2018-1-31	LDT	692	40
...	...	2018-1-31	LDT	880	50
12435889 – 1614351	LP 796-1	2017-4-15	LDT	red	...
13092185 – 2330350	CE 303	2017-4-16	LDT	blue	...
...	...	2017-4-16	LDT	red	...
14235017 – 1646116		2017-4-17	LDT	red	...
...	...	2018-1-31	LDT	880	50
15020759 + 7527526	LP 22-174	2017-4-13	LDT	red	...
...	...	2019-9-14	LDT	880	50
15085332 + 4934062		2017-4-13	LDT	red	...
...	...	2020-2-9	LDT	880	50
15211607 + 3945164	LP 222-70	2017-4-7	LDT	red	...
15263317 + 5522206	LP 135-316	2017-4-7	LDT	red	...
15434848 + 2552376	G 167-54	2017-4-12	LDT	blue	...
...	...	2017-4-12	LDT	red	...
15471513 + 0149218	LP 623-40	2017-4-15	LDT	red	...
16041322 + 2331386		2017-04-12	LDT	blue	...
...	...	2017-4-12	LDT	red	...
...	...	2017-5-4	LDT	red	...
17183572 + 0156433	Wolf 672 B	2017-4-9	LDT	blue	...
...	...	2017-4-9	LDT	red	...
17335314 + 1655129		2017-4-17	LDT	red	...
...	...	2019-9-13	LDT	880	50
18191622 – 0734518		2017-4-11	LDT	red	...
18523373 + 4538317	LHS 3420	2017-4-12	LDT	red	...
...	...	2019-9-13	LDT	880	50
20081786 + 3318122	GJ 1250	2019-9-14	LDT	880	50
21011610 + 3314328	L 1504-143	2017-10-21	LDT	692	40
...	...	2017-10-21	LDT	880	50
...	...	2018-8-2	WIYN	832	40
21134479 + 3634517		2018-8-29	WIYN	832	40
...	...	2019-9-13	LDT	880	50
22520522 – 1532511	LP 821-27	2019-9-14	LDT	880	50
23024353 + 7505591	LP 49-357	2019-1-20	WIYN	562	44
...	...	2019-1-20	WIYN	832	40

3. Results

Our observations of 1070 nearby M dwarfs revealed 145 known multiples and 26 previously undetected stellar companions. A future paper will present our detections of known multiples; here we present the new discoveries. In this section, we discuss systems that host both a new discovery and a known companion. We also report observed and astrophysical properties for the new discoveries; the observed properties were measured via our speckle observations, and the astrophysical properties were estimated using the observed properties as well as parallaxes from the literature.

3.1. Known Companions

Four of the 26 systems with new discoveries host known companions from the literature as well. This means that these systems are now trinary, or in the case of 2MASS J21011610+3314328, quaternary, as the B component of the system (2MASS J21012062+3314280) hosts a close-in stellar companion as well (Janson et al. 2014). Properties for the four systems with known companions are included in Table 2.

In the case of 2MASS J17183572+0156433, the known companion is a white dwarf. This system is discussed in detail in Section 4.1.

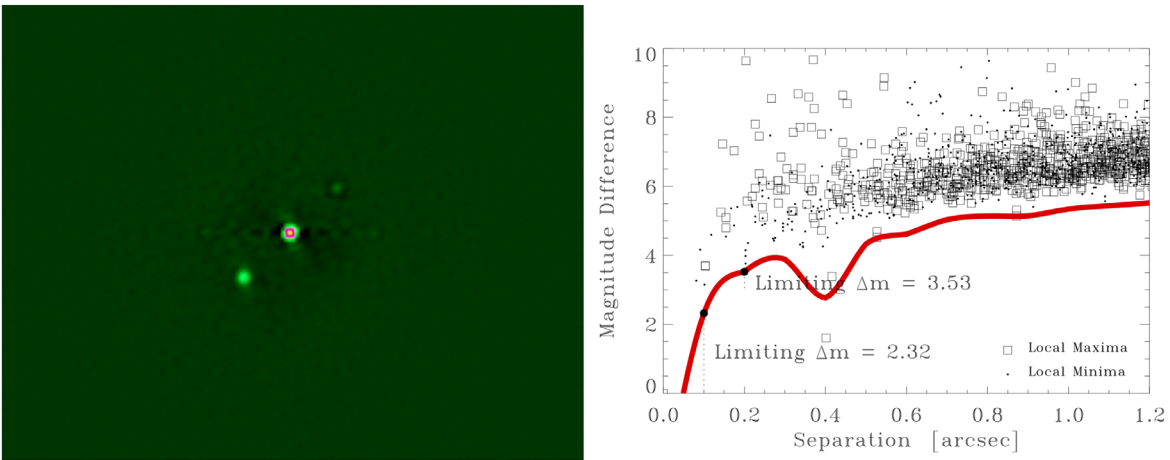


Figure 2. The newly detected companion to 2MASS J11030845+1517518, shown in the reconstructed image on the left and in the detection plot on the right. These data were taken on UT 2017 April 17. The companion is at a separation of $0''.39$ (6.8 au), and its delta magnitude is measured to be 1.5.

Table 2
Properties for Systems with a Previously Known Companion

2MASS ID	θ ($^\circ$)	ρ ($''$)	Δm	Reference
12190600 + 3150433	222	1.7	2.9	Lamman et al. (2020)
17183572 + 0156433	139	13	0.1	Luyten (1997)
21011610 + 3314328	95	57	0.9	Luyten (1997)
23024353 + 7505591	209	4.0	1.3	Luyten (1997)

3.2. New Discoveries

The observed properties for the new companions are reported in Table 3, where we have included the 2MASS ID of the primary, date of observation (measured in Besselian years), seeing, position angle (θ), angular separation (ρ), delta magnitude (Δm), and bandpass (λ). Again, for filterless observations, instead of listing the bandpass of the observation, we instead indicate whether the companion was detected in the “blue” ($\lambda \lesssim 700$ nm) image or the “red” ($\lambda \gtrsim 700$ nm) image. We also include entries for the known companion to 2MASS J12190600+3150433, since it was detected in our observations as well. The angular separation and delta magnitude distributions for the new discoveries are shown in Figure 3. A scatter plot of delta magnitude versus angular separation is shown in Figure 4.

We calculate residuals by computing the difference between the observed properties in each channel. The angular separation residuals have an average value of 3.4 mas, with a standard deviation of 6.5 mas. The position angle residuals have an average value of $0''.6$, with a standard deviation of $1''.0$. The delta magnitude residuals have an average value of 0.06, with a standard deviation of 0.23. The residuals result from the subtraction of two independent measurements with presumably the same uncertainty, so the subtraction has an uncertainty that is $\sqrt{2}$ larger than the uncertainty of either individual measure. This means that the uncertainty in a single angular separation measure is given by 6.5 mas divided by $\sqrt{2}$, or 4.6 mas. The average uncertainty in position angle is then $0''.7$, and the average uncertainty in delta magnitude is 0.16. When we take these values and add them in quadrature to the calibration uncertainties from Horch et al. (2021), we obtain values of 5.1 mas for the average angular separation uncertainty, $2''$ for

the average position angle uncertainty, and 0.21 for the average delta magnitude uncertainty. These uncertainties were propagated throughout our analysis described in Section 3.4. These values are slightly larger than those derived in Horch et al. (2017), Colton et al. (2021), or Horch et al. (2021); this is likely due to the faintness of our targets, and the filterless observations that took place during the 2017 April observing run. In general, filterless observations reduce the precision of our astrometry, but allow us to observe fainter companions.

3.3. Likelihood That the New Discoveries Are Bound

We note that it is highly unlikely these new discoveries are background stars due to the small fields-of-view of the instruments. We find that the number of stars brighter than $I = 15.5$ within a $2''$ area on the sky is ~ 0.0008 . This means that for our 26 detections, there is a $\sim 2.1\%$ chance that even a single detection is a random background star. Nonetheless, we investigate whether the new discoveries are bound in various ways.

First, Winters et al. (2019) list two of our targets found to host a new companion as suspected multiples in their work. In the case of the first suspected multiple, 2MASS J09510964-1219478, no astrometric parameters could be determined in the Double and Multiple Systems Annex (Lindgren et al. 1997), which could indicate that the star is actually a short-period astrometric binary. In the case of the second suspected multiple, Winters et al. (2019) used photometry from 2013 October to determine that 2MASS J20081786+3318122 is overluminous. We detected a companion to 2MASS J20081786+3318122 in 2019; there are therefore six years between the epochs of observation, which indicates that the object inducing this overluminosity is a common proper motion companion rather than a background contaminant.

We also assessed the boundedness of the new discoveries using second epoch observations. Because the targets in the POKEMON sample are nearby, they have high proper motions. Therefore, a second epoch observation can be taken to test the new discoveries for common proper motion with the target star. Ten of the 26 new discoveries have second epoch observations.

Additionally, we used the 2MASS identifiers of the targets found to have a new companion to find their Early Data Release 3 (EDR3; Gaia Collaboration 2021) identifiers, or in one case their Data Release 2 (DR2; Gaia Collaboration 2018)

Table 3
Observed Properties for Systems with a New Companion

2MASS ID	Date (2000+)	Seeing ($''$)	θ ($^{\circ}$)	ρ ($''$)	Δm	λ (nm)
03104962 – 1549408	17.8028	0.86	281.3	0.3577	1.68	880
03542561 – 0909316	17.8055	1.23	39.5	2.9997	3.04	880
07011725 + 1348085	17.2874	1.1	93.7	1.2858	1.67	red
07411976 + 6718444	17.2929	0.86	200.7	0.2085	0.70	red
09510964 – 1219478	17.3477	1.73	38.5	0.4497	3.30	880
11030845 + 1517518	17.2931	0.72	48.8	0.3912	1.42	blue
...	17.2931	0.81	48.1	0.3908	1.54	red
...	18.0851	0.70	44.4	0.3694	1.53	692
...	18.0851	0.68	43.9	0.3680	1.00	880
12190600 + 3150433	17.2931	0.66	331.8	0.1458	0.18	blue
...	17.2931	0.72	331.3	0.1415	0.09	red
...	18.0851	0.61	297.3	0.1287	0.01	692
...	18.0851	0.57	298.5	0.1253	0.01	880
...	17.2931	0.66	218.8	1.7697	5.54	blue
...	17.2931	0.72	222.9	1.6789	2.3	red
...	18.0851	0.61	216.5	1.6852	2.64	692
...	18.0851	0.57	218.7	1.6814	3.72	880
12435889 – 1614351	17.2876	0.91	284.7	0.3420	0.45	red
13092185 – 2330350	17.2906	0.63	105.1	1.1947	0.99	blue
...	17.2906	1.03	102.5	1.1752	1.03	red
14235017 – 1646116	17.2935	0.78	18.7	0.6604	3.29	red
...	18.0852	0.63	289.2	0.6039	2.57	880
15020759 + 7527526	17.2825	0.56	130.5	0.6188	2.39	red
...	19.7023	0.73	135.7	0.6256	0.56	880
15085332 + 4934062	17.2826	0.56	310.2	0.1574	1.50	red
...	20.1085	1.34	336.5	0.2655	1.66	880
15211607 + 3945164	17.2662	0.86	90.6	0.2378	0.78	red
15263317 + 5522206	17.2664	0.73	218.3	0.2280	1.13	red
15434848 + 2552376	17.2799	0.71	262.4	0.2448	0.31	blue
...	17.2799	0.75	262.0	0.2447	0.16	red
15471513 + 0149218	17.2881	0.73	287.0	0.2650	1.72	red
16041322 + 2331386	17.2800	0.63	109.0	0.1065	0.85	blue
...	17.2800	0.61	107.7	0.0982	0.37	red
...	17.3401	0.75	112.5	0.1018	0.45	red
17183572 + 0156433	17.2719	1.32	55.6	0.5307	1.05	blue
...	17.2719	1.28	55.0	0.5325	1.11	red
17335314 + 1655129	17.2938	0.69	101.0	0.1443	1.06	red
...	19.6995	1.05	62.6	0.3639	1.08	880
18191622 – 0734518	17.2775	0.74	132.9	0.5168	1.44	red
18523373 + 4538317	17.2802	0.81	37.7	0.4920	0.54	red
...	19.6995	0.99	28.7	0.4684	0.81	880
20081786 + 3318122	19.7026	0.69	237.6	0.4166	0.48	880
21011610 + 3314328	17.8048	1.39	348.7	0.2649	2.07	692
...	17.8048	1.19	347.8	0.2561	2.01	880
...	18.5853	1.15	355.2	0.2869	1.65	832
21134479 + 3634517	18.6600	0.65	10.6	0.3868	0.31	832
...	19.6995	1.15	5.5	0.3596	0.14	880
22520522 – 1532511	19.7027	0.60	252.4	0.7280	0.55	880
23024353 + 7505591	19.0532	0.81	3.0	0.4862	3.30	562
...	19.0532	0.63	3.7	0.4883	2.38	832

identifier, on the Gaia archive.⁷ If a secondary object was listed within $5''$ of the target, we calculated its angular separation from the target using its coordinates in Gaia. If the angular separation agreed with the separation we measured from our speckle observations, then we examined whether the parallaxes and proper motions of the secondary agreed with those of the primary to within 3σ . We determined that three of our new discoveries are bound using this methodology.

Moreover, nine of our 26 systems do not have parallaxes or proper motions listed in Gaia. This often occurs for close-in binary systems, as Gaia is unable to resolve the system, and the relative motion of the pair disrupts the parallax measurements. The absence of Gaia parallaxes or proper motions for these targets therefore suggests that the new discoveries we detected in these nine systems are indeed real.

Furthermore, Vrijmoet et al. (2020) notes that three out of four unresolved multistar red dwarf systems within 25 pc in Gaia DR2 have a parallax error larger than or equal to

⁷ <https://gea.esac.esa.int/archive>

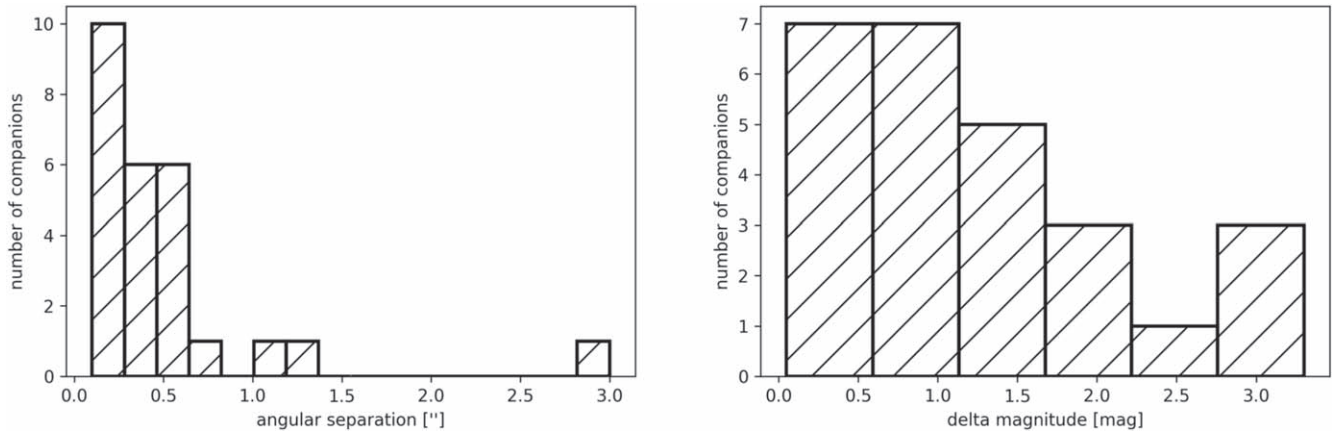


Figure 3. Angular separation (left) and I -band or “red” delta magnitude (right) distributions for the 26 new discoveries revealed by the POKEMON survey. These values were obtained from our DSSI and NESSI speckle observations, and have not been corrected for anisoplanatism.

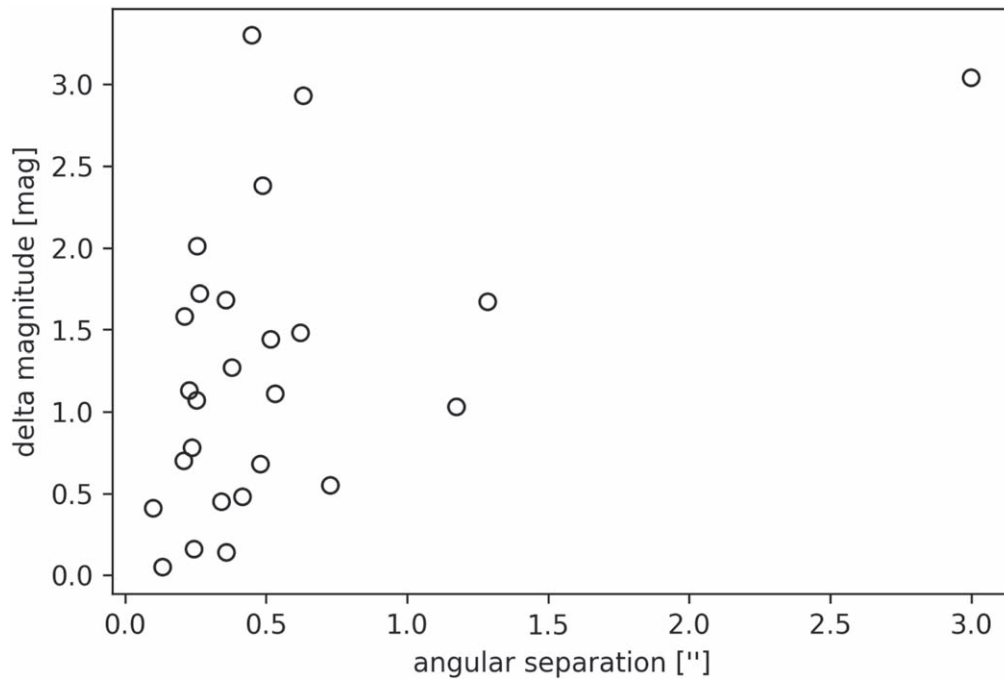


Figure 4. Scatter plot of delta magnitude versus angular separation for the 26 new discoveries. Most new discoveries are measured to be within $\sim 0.7''$ of their primaries, though they span a range of delta magnitudes.

0.32 mas, and parallaxes more than $\sim 10\%$ different than the long-term RECONS results. Thus, the large Gaia parallax errors for five of the targets found to have a new companion could be caused by the previously unresolved companions that we detected.

Finally, we examined the Gaia EDR3 renormalized unit weight error (RUWE) values associated with the targets found to have a new companion. The Gaia RUWE metric acts like a reduced chi-squared, where large values can indicate a poor model fit to the astrometry, assuming that the star is single. Single sources typically have RUWE values of ~ 1 , while sources with RUWE values > 1.4 are likely nonsingle or otherwise extended (Ziegler et al. 2020; Gaia Collaboration et al. 2021). Following Vrijmoet et al. (2020), which surveyed M dwarfs specifically, we use $\text{RUWE} > 2$ to distinguish single and (potentially) nonsingle sources, and find eight targets with elevated RUWE values.

In Table 4, we list the parallaxes and proper motions, as well as their errors and sources, for all targets found to have a new companion. We also include entries for the three new discoveries that appear in Gaia. 17 of the targets found to have a new companion have Gaia parallax estimates either from DR2 or EDR3. Parallaxes for the other nine primaries were obtained using the Fourth Edition of the General Catalogue of Trigonometric Stellar Parallaxes (YPC; van Altena et al. 1995), the MEarth survey (Dittmann et al. 2014), and the URAT Parallax Catalog (Finch et al. 2018). Proper motions were obtained either from Gaia or the fourth US Naval Observatory CCD Astrograph Catalog (UCAC4; Zacharias et al. 2012). We use * to note suspected multiples from Winters et al. (2019). We use † to note targets that have a second epoch observation. We use ‡ to note the new discoveries that appear in Gaia. We use § to note targets that do not have parallaxes or proper motions in Gaia EDR3. We

Table 4
Parallaxes and Proper Motions

2MASS ID	Parallax (mas)	Parallax Error (mas)	Parallax Source	Proper Motion (mas/yr)	Proper Motion Error (mas/yr)	Proper Motion Source	RUWE
03104962 – 1549408 ^{e,f}	23.2	0.7	Gaia EDR3	325.0, 0.9	0.6, 0.7	Gaia EDR3	12.8
03542561 – 0909316 ^c	47.41	0.02	Gaia EDR3	–95.41, 111.01	0.02, 0.02	Gaia EDR3	1.3
...	47.54	0.03	Gaia EDR3	–96.52, 99.07	0.03, 0.03	Gaia EDR3	1.9
07011725 + 1348085 ^c	24.52	0.04	Gaia EDR3	415.50, –97.40	0.05, 0.04	Gaia EDR3	1.1
...	24.1	0.1	Gaia EDR3	407.4, –96.4	0.2, 0.1	Gaia EDR3	2.8
07411976 + 6718444 ^f	41.5	0.3	Gaia EDR3	–110.3, –273.4	0.1, 0.2	Gaia EDR3	9.1
09510964 – 1219478 ^a	76.16	0.02	Gaia EDR3	1137.72, –1455.38	0.02, 0.01	Gaia EDR3	1.1
11030845 + 1517518 ^{b,d}	55	8	URAT	–419, –84	8, 8	UCAC4	...
12190600 + 3150433 ^b	35.20	0.08	Gaia EDR3	–295.61, 5.13	0.07, 0.08	Gaia EDR3	1.2
12435889 – 1614351 ^d	51	3	URAT	–422, 74	8, 8	UCAC4	...
13092185 – 2330350	66.60	0.1	Gaia EDR3	15.7, –383.77	0.1, 0.07	Gaia EDR3	1.0
14235017 – 1646116 ^b	16.93	0.03	Gaia EDR3	–108.81, –85.83	0.03, 0.02	Gaia EDR3	1.5
15020759 + 7527526 ^{b,d}	58	3	MEarth	–132, 160	8, 8	UCAC4	...
15085332 + 4934062 ^{b,f}	25.2	0.3	Gaia EDR3	–104.9, –13.3	0.3, 0.4	Gaia EDR3	27
15211607 + 3945164 ^d	45	1	MEarth	–436, 178	8, 8	UCAC4	...
15263317 + 5522206 ^d	42	4	MEarth	–111, 235	8, 8	UCAC4	...
15434848 + 2552376 ^d	45	2	MEarth	–171, 317	8, 8	UCAC4	...
15471513 + 0149218 ^{e,f}	56.4	0.4	Gaia EDR3	–213.4, –65.4	0.4, 0.3	Gaia EDR3	10
16041322 + 2331386 ^{b,f}	47.7	0.2	Gaia EDR3	–162.3, 16.9	0.1, 0.2	Gaia EDR3	9.8
17183572 + 0156433 ^{e,f}	27.8	0.4	Gaia EDR3	–447.5, –283.4	0.4, 0.3	Gaia EDR3	17
17335314 + 1655129 ^{b,e,f}	60.9	0.5	Gaia EDR3	–135.0, –130.5	0.5, 0.4	Gaia EDR3	16
18191622 – 0734518 ^d	10.4	0.3	Gaia DR2	–175.1, –213.5	0.6, 0.5	Gaia DR2	...
18523373 + 4538317 ^{b,d}	46	2	MEarth	206, 465	8, 8	UCAC4	...
20081786 + 3318122 ^{a,d}	46	5	YPC	340, 375	8, 8	UCAC4	...
21011610 + 3314328 ^{b,e,f}	49.8	0.7	Gaia EDR3	325.6, –164.2	0.6, 0.7	Gaia EDR3	37
21134479 + 3634517 ^{b,d}	51	2	URAT	–15.7, –92.3	6.5, 6.9	UCAC4	...
22520522 – 1532511	37.64	0.07	Gaia EDR3	331.41, 14.47	0.08, 0.07	Gaia EDR3	1.1
23024353 + 7505591 ^c	18.88	0.01	Gaia EDR3	285.23, 22.88	0.02, 0.02	Gaia EDR3	1.1
...	18.91	0.01	Gaia EDR3	286.33, 17.36	0.01, 0.02	Gaia EDR3	1.2

Notes.

- ^a Winters et al. (2019) suspected multiple.
^b Second epoch observation.
^c New discovery in Gaia.
^d No Gaia EDR3 parallax or proper motions.
^e Gaia parallax error > 0.32 mas.
^f RUWE > 2.

use || to note targets with a Gaia parallax error > 0.32 mas. Finally, we use # to note targets with RUWE > 2.

The only stars that do not have an indicator that they are nonsingle are 2MASS J13092185-2330350 and 2MASS J22520522-1532511. 2MASS J13092185-2330350 is a unique case where we obtained 46 data cubes on the same target because of its faintness, which could explain why its small and faint companion did not induce one of these indicators; this system is discussed further in Section 4.2. In the case of 2MASS J22520522-1532511, a secondary object does appear in Gaia EDR3, but it does not have a parallax or proper motions listed; this secondary object could potentially be the new discovery we detected.

3.4. Estimated Astrophysical Properties

Here we estimate projected separations, component masses and system mass ratios, and component spectral types for the 26 systems with new discoveries, assuming that there are no additional unknown components in each system (e.g., spectroscopic components).

We calculated projected separations for these 26 systems using our measured angular separations and the parallax estimates given in Table 4.

We then estimated mass ratios for these 26 systems using the empirical relationship between mass and luminosity (Delfosse et al. 2000; Benedict et al. 2016). This relationship was recently calibrated for late-type stars by Mann et al. (2019). Their code, which is publicly available on `github`,⁸ calculates a mass and its uncertainty given a user-provided distance and apparent K magnitude (and uncertainties). We calculated our distances using the parallaxes from Table 4, and obtained our K photometry from 2MASS (Skrutskie et al. 2006). However, the resolution for 2MASS is estimated to be $5''$, and all of the new companions detected throughout this survey are within $5''$ of their primary stars. This means that the 2MASS K magnitudes for these systems convolve the flux from both the primary and secondary stars. In order to separate the 2MASS K magnitudes into their component parts, we first estimated a K -band delta magnitude using the method outlined by Lamman et al. (2020). For this we used our measured speckle I -band delta magnitude, or the “red” delta magnitude in the case of the filterless observations, and the PARSEC theoretical stellar evolution models (Marigo et al. 2017).

⁸ https://github.com/awmann/M_-M_K-

We then derived two equations to solve for the K magnitude of the primary and secondary stars. For this we used the K -band delta magnitude and the 2MASS K magnitude of the primary star.

The first equation we derived is simply the difference between the secondary K magnitude and the primary K magnitude:

$$\Delta K = K_2 - K_1. \quad (1)$$

The second equation originated from the equation for apparent magnitude, which is defined as a logarithmic luminosity ratio of a body to some standard.

$$m = -2.5 \log_{10} \left(\frac{L}{L_0} \right). \quad (2)$$

The combined apparent magnitude of the binary system can then be written as

$$m_{\text{binary}} = -2.5 \log_{10} \left(\frac{L_{\text{binary}}}{L_0} \right) \quad (3)$$

where

$$\frac{L_{\text{binary}}}{L_0} = \frac{L_1}{L_0} + \frac{L_2}{L_0} = 10^{-m_1/2.5} + 10^{-m_2/2.5}. \quad (4)$$

Our second equation is therefore

$$K_{\text{binary}} = -2.5 \log_{10} (10^{-K_1/2.5} + 10^{-K_2/2.5}). \quad (5)$$

We then used the `scipy.optimize` subpackage (Virtanen et al. 2020) to solve Equations (1) and (5) for our two unknowns: the K magnitude of the primary and the K magnitude of the secondary.

When observing 2MASS J12190600+3150433, we detected the companion known to the literature in addition to the new discovery. Therefore, to calculate the component K magnitudes for this system, we used an additional equation to calculate the K -band delta magnitude for the tertiary in the system, and added a $10^{-K_3/2.5}$ term to Equation (5).

Once we obtained a K magnitude for each component in a given system, we were able to estimate the component masses and calculate a mass ratio for the system. We note that the relationship between mass and luminosity only behaves for main-sequence stars; in the case of pre-main-sequence stars, their ages must be known and accounted for as well. The M dwarfs, and in particular the later spectral subtypes, have extensive pre-main-sequence phases. Therefore, the masses for young members of our sample could be estimated incorrectly if their ages are unknown. Winters et al. (2019) finds 17 known young members in their sample of 1120 nearby M dwarfs. Six of these are in our sample as well; however, none of these young stars host a new discovery.

We also determined component spectral types using the component masses we obtained, as well as reference stellar masses and spectral types⁹ (Pecaut et al. 2012; Pecaut & Mamajek 2013). We note that this is a coarse method for estimating spectral types; we are therefore currently using the Titan Monitor (TiMo) facility at Lowell Observatory to obtain homogeneous spectral types for the entire POKEMON sample.

The projected separations, mass ratios, and component spectral types for these 26 systems are reported in Table 5. We also include an entry for the known companion to 2MASS J12190600+3150433, since it was detected in our observations as well.

We note that for some of the 26 stars with new companions, multiplying their seeing value by their separation value from Table 3 produces a value larger than $0''.6$ squared. As shown in previous LDT speckle papers (Horch et al. 2015, 2020), a value larger than $0''.6$ squared could indicate that the photometry has a systematic error, which could make the values listed in Table 5 unreliable. We note these systems with an asterisk.

We note that our spectral type estimates for 2MASS J14235017-1646116 and 2MASS J23024353+7505591 are K8 and K5, respectively. Kirkpatrick et al. (2016) lists 2MASS J14235017-1646116 as a M0.5 star, but 2MASS J23024353+7505591 does not have a spectral type listed in the literature. In order to confirm our spectral type estimates, one would need to obtain low-resolution spectroscopy of these objects, which is outside the scope of this work. However, we are in the process of following up POKEMON targets with the TiMo facility at Lowell Observatory.

4. Discussion

Here we discuss a new companion in a system with both a known M dwarf and a known white dwarf, a potential brown dwarf binary, and initial insights from the POKEMON survey.

4.1. A Triple System with a Known White Dwarf

As noted in Section 3.2, four of the 26 systems with new discoveries also host companions known to the literature. The companion to 2MASS J17183572+0156433, called Wolf 672 A, is a known white dwarf (Gianninas et al. 2011).

This system was excluded from the final POKEMON sample, since all systems with primaries more massive than M dwarfs have now been removed. We also do not include this system in our calculation of the M-dwarf multiplicity or companion rates. Nonetheless, we note here the discovery of a new M-dwarf companion in this system, which makes the system trinary.

Systems that include both an M dwarf and a white dwarf are critical to our understanding of M dwarfs, as our low-mass neighbors are notoriously difficult to model, whereas the white dwarfs have a well-defined chain of models (Fontaine et al. 2001) that can be used to estimate the age of their main-sequence companion (Garcés et al. 2011; Kiman et al. 2021). This estimation of ages using white dwarfs can have uncertainties as low as 10%–20% (Fouesneau et al. 2019). White dwarf/M dwarf systems can also be used to study mass loss (Debes 2006). This system is therefore of particular interest for understanding the formation and evolution of the M-dwarf companions.

Wolf 672 A is included in the Montreal White Dwarf Database,¹⁰ where its effective temperature and $\log g$ are listed as 12461 ± 113 and 7.89 ± 0.01 , respectively. Using these parameters, the fact that the Montreal White Dwarf Database lists Wolf 672 A as a dA white dwarf, and the `wdwarfdate` code (Choi et al. 2016; Dotter 2016; Cummings et al. 2018; Bédard et al. 2020; Kiman et al. 2022) that is publicly available

⁹ “A Modern Mean Dwarf Stellar Color and Effective Temperature Sequence,” http://www.pas.rochester.edu/~mamajek/EEM_dwarf_UBVIJHK_colors_Teff.txt.

¹⁰ <https://www.montrealwhitedwarfdatabase.org>

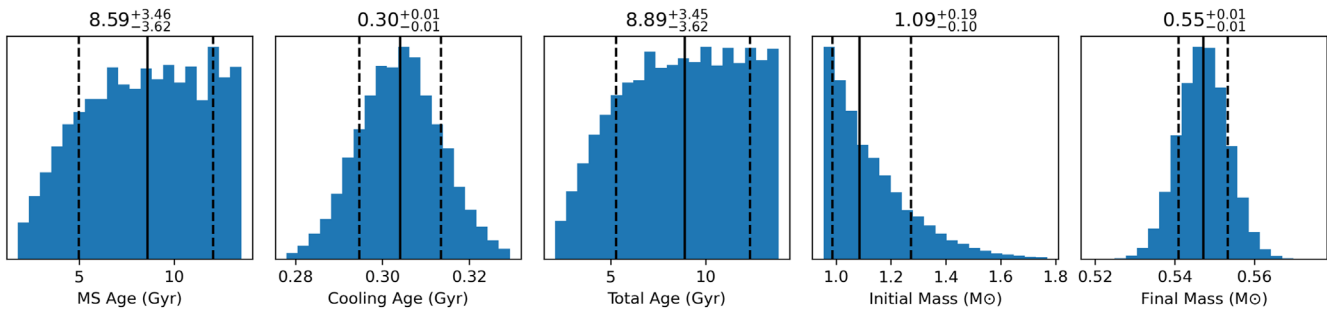


Figure 5. Using the `wdwarfdate` code, we estimate an age for the white dwarf Wolf 672 A, and thus its companions, the M dwarf Wolf 672 B and the new discovery we detected. The panels (from left to right) show the main-sequence age (the age of the progenitor), the cooling age, the total age, the initial mass (the mass of the progenitor), and the final mass of the white dwarf. We find a cooling age of $0.30^{+0.01}_{-0.01}$ Gyr, and a final mass of $0.55^{+0.01}_{-0.01} M_{\odot}$, which are in complete agreement with the Montreal White Dwarf Database values for Wolf 672 A of 0.29 Gyr and $0.55 M_{\odot}$.

Table 5
Estimated Astrophysical Properties for Systems with a New Companion

2MASS ID	Projected Separation (au)	Primary Mass (M_{\odot})	Companion Mass (M_{\odot})	Mass Ratio	Primary Spectral Type	Companion Spectral Type
03104962 – 1549408	15.4 ± 0.6	0.29 ± 0.03	0.15 ± 0.01	0.53 ± 0.09	M3	M5
03542561 – 0909316 ^a	63.28 ± 0.04	0.54 ± 0.03	0.19 ± 0.02	0.35 ± 0.05	M0.5	M4
07011725 + 1348085 ^a	52.4 ± 0.1	0.30 ± 0.03	0.16 ± 0.01	0.53 ± 0.09	M3	M5
07411976 + 6718444	5.0 ± 0.2	0.15 ± 0.01	0.120 ± 0.008	0.8 ± 0.1	M5	M5.5
09510964 – 1219478 ^a	5.90 ± 0.08	0.50 ± 0.03	0.16 ± 0.01	0.31 ± 0.04	M0.5	M5
11030845 + 1517518	7 ± 1	0.28 ± 0.05	0.17 ± 0.03	0.6 ± 0.2	M3	M4.5
12190600 + 3150433 ^a	3.8 ± 0.3	0.46 ± 0.03	0.45 ± 0.03	1.0 ± 0.1	M1.5	M1.5
	47.7 ± 0.1	0.46 ± 0.03	0.15 ± 0.01	0.33 ± 0.05	M1.5	M5
12435889 – 1614351	6.7 ± 0.5	0.17 ± 0.02	0.15 ± 0.02	0.86 ± 0.2	M4.5	M5
13092185 – 2330350 ^a	17.65 ± 0.06	0.082 ± 0.004	0.076 ± 0.003	0.93 ± 0.08	M8	L1
14235017 – 1646116	37.3 ± 0.1	0.59 ± 0.03	0.23 ± 0.02	0.39 ± 0.05	K8	M3.5
15020759 + 7527526	10.7 ± 0.5	0.114 ± 0.007	0.086 ± 0.004	0.76 ± 0.08	M5.5	M7.5
15085332 + 4934062	8.4 ± 0.3	0.51 ± 0.03	0.31 ± 0.03	0.60 ± 0.08	M0.5	M3
15211607 + 3945164	5.3 ± 0.3	0.14 ± 0.01	0.113 ± 0.007	0.8 ± 0.1	M5	M5.5
15263317 + 5522206	5.5 ± 0.7	0.15 ± 0.02	0.11 ± 0.01	0.7 ± 0.2	M5	M5.5
15434848 + 2552376	5.5 ± 0.4	0.16 ± 0.01	0.16 ± 0.01	0.9 ± 0.2	M4.5	M5
15471513 + 0149218	4.9 ± 0.2	0.130 ± 0.008	0.091 ± 0.004	0.70 ± 0.08	M5	M6.5
16041322 + 2331386	2.1 ± 0.4	0.17 ± 0.01	0.15 ± 0.01	0.9 ± 0.1	M4.5	M5
17183572 + 0156433 ^a	19.1 ± 0.3	0.35 ± 0.03	0.22 ± 0.02	0.6 ± 0.1	M3	M3.5
17335314 + 1655129	4.2 ± 0.2	0.25 ± 0.02	0.16 ± 0.01	0.7 ± 0.1	M3.5	M4.5
18191622 – 0734518	50 ± 1	0.52 ± 0.03	0.33 ± 0.03	0.64 ± 0.09	M0.5	M3
18523373 + 4538317	10.4 ± 0.6	0.14 ± 0.01	0.115 ± 0.008	0.8 ± 0.1	M5	M5.5
20081786 + 3318122	9 ± 1	0.18 ± 0.03	0.15 ± 0.02	0.8 ± 0.2	M4.5	M5
21011610 + 3314328	5.1 ± 0.2	0.40 ± 0.03	0.18 ± 0.02	0.46 ± 0.08	M2.5	M4.5
21134479 + 3634517	7.1 ± 0.3	0.18 ± 0.02	0.17 ± 0.02	0.9 ± 0.2	M4.5	M4.5
22520522 – 1532511	19.34 ± 0.09	0.20 ± 0.02	0.16 ± 0.01	0.8 ± 0.1	M4	M5
23024353 + 7505591	25.87 ± 0.09	0.67 ± 0.02	0.41 ± 0.02	0.62 ± 0.05	K5	M2

Note.

^a Seeing $\times \rho > 0''.6$ squared.

on [github](https://github.com/rkiman/wdwarfdate),¹¹ we estimate an age for the white dwarf Wolf 672 A, and thus its companions, the M dwarf Wolf 672 B and the new discovery we detected (Figure 5). We find an age for this system of $8.89^{+3.45}_{-3.62}$ Gyr, demonstrating the utility of observing white-dwarf/M-dwarf systems.

4.2. A Potential Brown Dwarf Companion

As noted in Section 2.2, during our observing run in 2017 April, the narrowband speckle filters were not installed within DSSI. Although these filters produce more contrast in the

speckles, a large portion of the photons gathered by the telescope remain unused. Filterless observing could thus be beneficial for probing new speckle imaging discovery space, such as in the case of 2MASS J13092185-2330350.

2MASS J13092185-2330350 is listed as an M7 star (Gizis 2002), and has a magnitude of 18.0 in the *R* band (Reid et al. 2007). On UT April 16 2017, we obtained 46 data cubes for 2MASS J13092185-2330350, rather than the standard nine, using DSSI at the 4.3 m LDT. These observations were taken at the end of the night, which was an opportunity to test the possibility of observing systems beyond the faint limit of DSSI. As shown in Section 3.2, these observations revealed a companion in both channels, at $1''.1947$ and with a delta

¹¹ <https://github.com/rkiman/wdwarfdate>

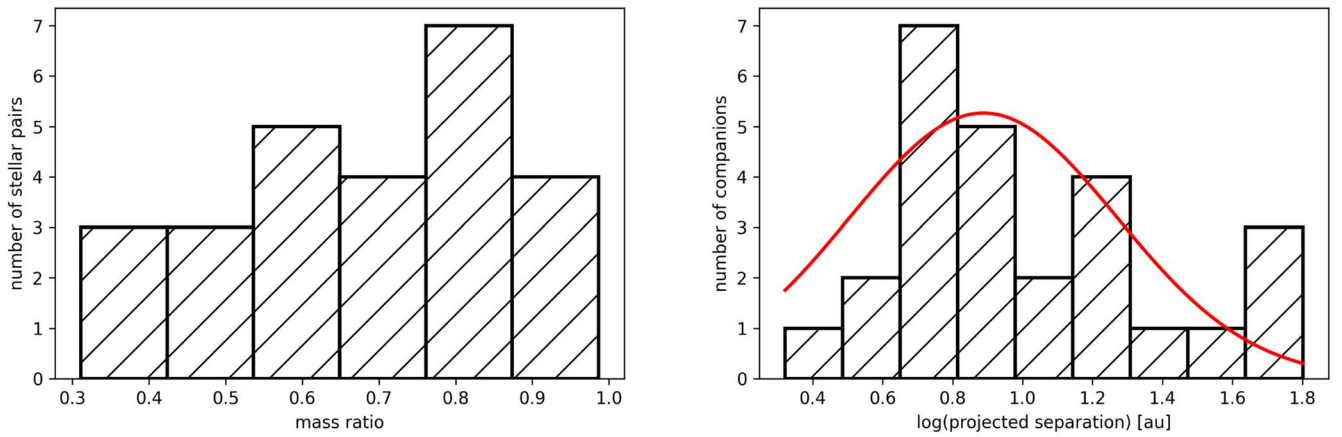


Figure 6. The mass ratio (left) and projected separation (right) distributions for the 26 previously undetected companions discovered throughout the POKEMON survey. These values were estimated using our observed properties, as well as the parallaxes and 2MASS K magnitudes for these objects. The mass ratios follow a relatively flat distribution, while the projected separations follow a roughly Gaussian distribution, as expected. The peak of our projected separation distribution is at 7.8 au, with a standard deviation of $\sigma_{\log a} = 0.4$.

magnitude of 0.99 at 692 nm, and at $1''.1752$ and with a delta magnitude of 1.03 at 880 nm. According to our analysis described in Section 3.4, the projected separation for this new companion is 17.64 au. The mass of the primary is $0.082 M_{\odot}$, and the mass of the secondary is $0.076 M_{\odot}$, corresponding to a mass ratio of 0.926. We estimate that the spectral type of the primary is M8, and that the spectral type of the secondary is L1, making the secondary a potential brown dwarf. In order to confirm these spectral types, one would need to obtain low-resolution spectroscopy of these objects; this is outside the scope of this work, though we are currently following up POKEMON targets with the TiMo facility at Lowell Observatory. In any case, this system provides an argument for further investigation into filterless speckle observations, as well as systems beyond the faint limit of the instruments.

4.3. Initial Insights from the POKEMON Survey

Though the full analysis of the POKEMON sample has yet to be published, we discuss here initial insights that can be made about the POKEMON sample based on the 26 newly discovered companions.

As shown in Figure 3, almost all of the angular separations we measured are within $\sim 0''.7$, and the smallest angular separation was measured to be $0''.0982$. There are also new companions with delta magnitudes as large as 3.30. We note that these distributions have not been completeness-corrected. Therefore close companions at large delta magnitudes would be preferentially missed, since the sensitivity of the instruments decreases with decreasing separation. Additionally, wide companions would be preferentially missed due to the small field-of-views of the instruments, or preferentially excluded since many wide companions have been detected by previous surveys. Nonetheless, the small angular separations and the large range of delta magnitudes of the new discoveries discussed here explain why speckle imaging was needed to detect these 26 new companions.

In Figure 6, we show the mass ratio and projected separation distributions for the 26 new companions. The mass ratios follow a relatively flat distribution, while the logarithms of the projected separations follow a roughly Gaussian distribution. The peak of our projected separation distribution is at 7.8 au with a standard deviation of $\sigma_{\log a} = 0.4$. The sample that

generated these distributions is of course small; the statistics on these distributions will become more robust once all detections from the full POKEMON survey are included. Nonetheless, our peak is comparable to that of Winters et al. (2019), which found a peak at 20 au for their sample of M dwarfs within 25 pc, and at 4 au for M dwarfs within 10 pc. In contrast, Raghavan et al. (2010) found a peak at 51 au for solar-type stars within 25 pc. It is telling that though we used a different technique than Winters et al. (2019) to probe M-dwarf multiplicity, our projected separation distributions are consistent with one another, and are not consistent with the distribution from Raghavan et al. (2010); these results demonstrate the differences between the stellar companions that M dwarfs host, and those that solar-type stars host.

There are 1070 M dwarfs in the POKEMON sample; 290 of these are currently known to host at least one stellar companion. We discovered 26 new companions throughout this survey; 22 of these were discovered in systems that were previously thought to be single. These 22 new discoveries therefore increase the number of M dwarfs in the POKEMON sample with a known companion by 7.6%. Though we have not yet performed sufficient analysis to determine an updated M-dwarf multiplicity rate, these new discoveries increase the companion fraction from 27.1%, which is in agreement with Winters et al. (2019), to 29.2%—a 2.1% percentage units increase. This increase demonstrates that it is critical to survey our M-dwarf neighbors with high-resolution imaging in order to search for stellar companions within $2''$, and to fully understand M-dwarf multiplicity.

5. Conclusions and Future Work

We have carried out the POKEMON speckle survey of nearby M dwarfs, which is volume-limited through M9, out to at least 15 pc, with additional brighter targets at larger distances. The POKEMON survey has resulted in observations of 1070 M dwarfs at large-telescope, diffraction-limited resolution. These observations have revealed 26 new companions to these objects.

We used our observed properties, parallaxes from the literature, and the targets' 2MASS K magnitudes to estimate astrophysical properties for these objects including projected separation, mass ratio, and component spectral types.

We report the discovery of a new companion in a system with both a known M dwarf and a known white dwarf, and discuss a new companion that is a potential brown dwarf. We also explore initial insights from the POKEMON survey.

In a forthcoming publication, we will present the full POKEMON survey, as well as an updated M-dwarf multiplicity rate, calculated by spectral subtype through M9 for the first time. We are also currently carrying out a follow up of the targets in the POKEMON sample in various ways. First, we are using the Titan Monitor facility at Lowell Observatory to obtain homogeneous spectral types for the entire POKEMON sample. Additional follow-up observing is being pursued with the Quad-camera Wavefront-sensing Six-channel Speckle Interferometer (QWSSI; Clark et al. 2020), which was commissioned at the LDT in 2020 July. While DSSI and NESSI image at two visible wavelengths, QWSSI observes at four channels in the optical, as well as two in the near-infrared, and also includes simultaneous wave front sensing. Because the M dwarfs emit most strongly in the near-infrared, QWSSI will aid us in measuring the multiplicity of the late-type M dwarfs that were unable to be explored by the previous-generation speckle imagers. This new capability will allow us to build on the POKEMON survey and develop a more complete picture of M-dwarf multiplicity for the later subtypes, and potentially even the L and T dwarfs.

We thank our anonymous reviewer for their thoughtful assessment. We also thank Frederick Hahne, Zachary Hartman, and Joe Llama for their contributions to and feedback on this manuscript. Finally, we thank the army of TOs at the LDT and the WIYN Telescope for all of their help and insight during our 50 nights of observing.

This research was supported by NSF grant No. AST-1616084 and JPL RSA No. 1610345.

These results made use of the Lowell Discovery Telescope at Lowell Observatory. Lowell is a private, nonprofit institution dedicated to astrophysical research and public appreciation of astronomy and operates the LDT in partnership with Boston University, the University of Maryland, the University of Toledo, Northern Arizona University, and Yale University. Lowell Observatory sits at the base of mountains sacred to tribes throughout the region. We honor their past, present, and future generations, who have lived here for millennia and will forever call this place home.

These results are also based on observations from Kitt Peak National Observatory, the NSF's National Optical-Infrared Astronomy Research Laboratory (NOIRLab Prop. ID: 2018B-0126; PI: C. Clark), which is operated by the Association of Universities for Research in Astronomy (AURA) under a cooperative agreement with the National Science Foundation. Data presented herein were obtained at the WIYN Observatory from telescope time allocated to NN-EXPLORE through the scientific partnership of the National Aeronautics and Space Administration, the National Science Foundation, and the NSF's National Optical-Infrared Astronomy Research Laboratory.

This work presents results from the European Space Agency (ESA) space mission Gaia. Gaia data are being processed by the Gaia Data Processing and Analysis Consortium (DPAC). Funding for the DPAC is provided by national institutions, in particular the institutions participating in the Gaia MultiLateral Agreement (MLA). The Gaia mission website is [https://www.](https://www.cosmos.esa.int/gaia)

[cosmos.esa.int/gaia](https://archives.esac.esa.int/gaia). The Gaia archive website is <https://archives.esac.esa.int/gaia>.


This work has used data products from the Two Micron All Sky Survey (Skrutskie et al. 2019), which is a joint project of the University of Massachusetts and the Infrared Processing and Analysis Center at the California Institute of Technology, funded by NASA and NSF.

Information was collected from several additional large database efforts: the Simbad database and the VizieR catalog access tool, operated at CDS, Strasbourg, France; NASA's Astrophysics Data System; the Washington Double Star Catalog maintained at the US Naval Observatory; and the fourth US Naval Observatory CCD Astrograph Catalog (Zacharias et al. 2020).

Facilities: LDT(DSSI), WIYN(NESSI).

Software: Astropy (Astropy Collaboration et al. 2013), IPython (Pérez & Granger 2007), Matplotlib (Hunter 2007), NumPy (Harris et al. 2020), Pandas (McKinney et al. 2010), SciPy (Virtanen et al. 2020).

ORCID iDs

Catherine A. Clark  <https://orcid.org/0000-0002-2361-5812>
Gerard T. van Belle  <https://orcid.org/0000-0002-8552-158X>
Elliott P. Horch  <https://orcid.org/0000-0003-2159-1463>
Kaspar von Braun  <https://orcid.org/0000-0002-5823-4630>
David R. Ciardi  <https://orcid.org/0000-0002-5741-3047>
Jennifer G. Winters  <https://orcid.org/0000-0001-6031-9513>
Rocio Kiman  <https://orcid.org/0000-0003-2102-3159>

References

- Alonso-Floriano, F. J., Morales, J. C., Caballero, J. A., et al. 2015, *A&A*, **577**, A128
- Astropy Collaboration, Robitaille, T. P., Tollerud, E., et al. 2013, *A&A*, **558**, A33
- Baraffe, I., & Chabrier, G. 1996, *ApJL*, **461**, L51
- Bédard, A., Bergeron, P., Brassard, P., & Fontaine, G. 2020, *ApJ*, **901**, 93
- Benedict, G. F., Henry, T. J., Franz, O. G., et al. 2016, *AJ*, **152**, 141
- Bergfors, C., Brandner, W., Daengen, S., et al. 2013, *MNRAS*, **428**, 182
- Borucki, W. J., Koch, D. G., Basri, G., et al. 2011, *ApJ*, **728**, 117
- Bouma, L. G., Masuda, K., & Winn, J. N. 2018, *AJ*, **155**, 244
- Choi, J., Dotter, A., Conroy, C., et al. 2016, *ApJ*, **823**, 102
- Ciardi, D. R., Beichman, C. A., Horch, E. P., & Howell, S. B. 2015, *ApJ*, **805**, 16
- Clark, C. A., van Belle, G. T., Ciardi, D. R., et al. 2022, *AJ*, **163**, 232
- Clark, C. A., van Belle, G. T., Horch, E. P., et al. 2020, *Proc. SPIE*, **11446**, 114462A
- Colton, N. M., Horch, E. P., Everett, M. E., et al. 2021, *AJ*, **161**, 21
- Cummings, J. D., Kalirai, J. S., Tremblay, P. E., Ramirez-Ruiz, E., & Choi, J. 2018, *ApJ*, **866**, 21
- Debes, J. H. 2006, *ApJ*, **652**, 636
- Delfosse, X., Forveille, T., Ségransan, D., et al. 2000, *A&A*, **364**, 217
- Deshpande, R., Blake, C. H., Bender, C. F., et al. 2013, *AJ*, **146**, 156
- Dittmann, J. A., Irwin, J. M., Charbonneau, D., & Berta-Thompson, Z. K. 2014, *ApJ*, **784**, 156
- Dotter, A. 2016, *ApJS*, **222**, 8
- Duchêne, G., & Kraus, A. 2013, *ARA&A*, **51**, 269
- Dupuy, T. J., & Liu, M. C. 2012, *ApJS*, **201**, 19
- Finch, C. T., Zacharias, N., & Jao, W.-C. 2018, *AJ*, **155**, 176
- Fontaine, G., Brassard, P., & Bergeron, P. 2001, *PASP*, **113**, 409
- Fontanive, C., & Bardalez Gagliuffi, D. 2021, *FrASS*, **8**, 16
- Fontanive, C., Rice, K., Bonavita, M., et al. 2019, *MNRAS*, **485**, 4967
- Fouesneau, M., Rix, H.-W., von Hippel, T., Hogg, D. W., & Tian, H. 2019, *ApJ*, **870**, 9
- Furlan, E., & Howell, S. B. 2020, *ApJ*, **898**, 47
- Gaia Collaboration, Brown, A. G. A., Vallenari, A., et al. 2018, *A&A*, **616**, A1
- Gaia Collaboration, Brown, A. G. A., Vallenari, A., et al. 2021, *A&A*, **649**, A1
- Garcés, A., Catalán, S., & Ribas, I. 2011, *A&A*, **531**, A7

- Gianninas, A., Bergeron, P., & Ruiz, M. T. 2011, *ApJ*, 743, 138
- Gizis, J. E. 2002, *ApJ*, 575, 484
- Gliese, W., & Jahreiß, H. 1991, Preliminary Version of the Third Catalogue of Nearby Stars, On: The Astronomical Data Center CD-ROM: Selected Astronomical Catalogs
- Haghighipour, N., & Raymond, S. N. 2007, *ApJ*, 666, 436
- Harris, C. R., Millman, K. J., van der Walt, S. J., et al. 2020, *Natur*, 585, 357
- Hartkopf, W. I., Mason, B. D., & Worley, C. E. 2001, *AJ*, 122, 3472
- Henry, T. J., Jao, W.-C., Subasavage, J. P., et al. 2006, *AJ*, 132, 2360
- Hirsch, L. A., Ciardi, D. R., Howard, A. W., et al. 2017, *AJ*, 153, 117
- Hirsch, L. A., Rosenthal, L., Fulton, B. J., et al. 2021, *AJ*, 161, 134
- Hoffleit, D., & Jaschek, C. 1982, The Bright Star Catalogue. Fourth revised edition. (Containing data compiled through 1979). (Washington, DC: NASA)
- Horch, E. P., Gomez, S. C., Sherry, W. H., et al. 2011a, *AJ*, 141, 45
- Horch, E. P., van Altena, W. F., Howell, S. B., Sherry, W. H., & Ciardi, D. R. 2011b, *AJ*, 141, 180
- Horch, E. P., van Belle, G. T., Davidson, J. W. J., et al. 2015, *AJ*, 150, 151
- Horch, E. P., Veillette, D. R., Baena Gallé, R., et al. 2009, *AJ*, 137, 5057
- Horch, E. P., Casetti-Dinescu, D. I., Camarata, M. A., et al. 2017, *AJ*, 153, 212
- Horch, E. P., van Belle, G. T., Davidson, J. W. J., et al. 2020, *AJ*, 159, 233
- Horch, E. P., Broderick, K. G., Casetti-Dinescu, D. I., et al. 2021, *AJ*, 161, 295
- Howell, S. B. 2020, *FrASS*, 7, 10
- Howell, S. B., Matson, R. A., Ciardi, D. R., et al. 2021, *AJ*, 161, 164
- Howell, S. B., Sobek, C., Haas, M., et al. 2014, *PASP*, 126, 398
- Hunter, J. D. 2007, *CSE*, 9, 90
- Jang-Condell, H. 2015, *ApJ*, 799, 147
- Janson, M., Hormuth, F., Bergfors, C., et al. 2012, *ApJ*, 754, 44
- Janson, M., Bergfors, C., Brandner, W., et al. 2014, *ApJS*, 214, 17
- Kimani, R., Faherty, J. K., Cruz, K. L., et al. 2021, *AJ*, 161, 277
- Kimani, R., Xu, S., & Faherty, J. K. 2022, arXiv:2206.05388
- Kirkpatrick, J. D., Schneider, A., Fajardo-Acosta, S., et al. 2014, *ApJ*, 783, 122
- Kirkpatrick, J. D., Kellogg, K., Schneider, A. C., et al. 2016, *ApJS*, 224, 36
- Kraus, A. L., Ireland, M. J., Hillenbrand, L. A., & Martinache, F. 2012, *ApJ*, 745, 19
- Kraus, A. L., Ireland, M. J., Huber, D., Mann, A. W., & Dupuy, T. J. 2016, *AJ*, 152, 8
- Labeyrie, A. 1970, *A&A*, 6, 85
- Lamman, C., Baranec, C., Berta-Thompson, Z. K., et al. 2020, *AJ*, 159, 139
- Laughlin, G., Bodenheimer, P., & Adams, F. C. 1997, *ApJ*, 482, 420
- Lester, K. V., Matson, R. A., Howell, S. B., et al. 2021, *AJ*, 162, 75
- Lindgren, L., Mignard, F., Söderhjelm, S., et al. 1997, *A&A*, 323, L53
- Lohmann, A. W., Weigelt, G., & Wimitzer, B. 1983, *ApOpt*, 22, 4028
- López-Morales, M., Ben-Ami, S., Gonzalez-Abad, G., et al. 2019, *AJ*, 158, 24
- Luhman, K. L., & Sheppard, S. S. 2014, *ApJ*, 787, 126
- Luyten, W. J. 1997, VizieR Online Data Catalog I/130
- Magnier, E. A., Liu, M. C., Aller, K., Best, W., & Deacon, N. 2015, *IAUGA*, 29, 2257922
- Mann, A. W., Dupuy, T., Kraus, A. L., et al. 2019, *ApJ*, 871, 63
- Marigo, P., Girardi, L., Bressan, A., et al. 2017, *ApJ*, 835, 77
- Mason, B. D., Hartkopf, W. I., Gies, D. R., Henry, T. J., & Helsel, J. W. 2009, *AJ*, 137, 3358
- McKinney, W., et al. 2010, in Proc. of the 9th Python in Science Conf., Vol. 445 (Austin, TX: SciPy), 51
- Moe, M., & Kratter, K. M. 2021, *MNRAS*, 507, 3593
- Mustill, A. J., Lambrechts, M., & Davies, M. B. 2022, *A&A*, 658, A199
- Pecaut, M. J., & Mamajek, E. E. 2013, *ApJS*, 208, 9
- Pecaut, M. J., Mamajek, E. E., & Bubar, E. J. 2012, *ApJ*, 746, 154
- Pérez, F., & Granger, B. E. 2007, *CSE*, 9, 21P
- Rafikov, R. R., & Silsbee, K. 2015a, *ApJ*, 798, 69
- Rafikov, R. R., & Silsbee, K. 2015b, *ApJ*, 798, 70
- Raghavan, D., McAlister, H. A., Henry, T. J., et al. 2010, *ApJS*, 190, 1
- Reid, I. N., Cruz, K. L., & Allen, P. R. 2007, *AJ*, 133, 2825
- Ricker, G. R., Winn, J. N., Vanderspek, R., et al. 2015, *JATIS*, 1, 014003
- Scott, N. J., Howell, S. B., Horch, E. P., & Everett, M. E. 2018, *PASP*, 130, 054502
- Skrutskie, M. F., Cutri, R. M., Stiening, R., et al. 2006, *AJ*, 131, 1163
- Skrutskie, M. F., Cutri, R. M., Stiening, R., et al. 2019, 2MASS All-Sky Point Source Catalog, IPAC, doi:10.26131/IRSA2
- Su, X.-N., Xie, J.-W., Zhou, J.-L., & Thebault, P. 2021, *AJ*, 162, 272
- Teske, J. K., Ciardi, D. R., Howell, S. B., Hirsch, L. A., & Johnson, R. A. 2018, *AJ*, 156, 292
- van Altena, W. F., Lee, J. T., & Hoffleit, E. D. 1995, The general catalogue of trigonometric [stellar] parallaxes (New Haven, CT: Yale Univ. Observatory)
- Virtanen, P., Gommers, R., Oliphant, T. E., et al. 2020, *NatMe*, 17, 261
- Vrijmoet, E. H., Henry, T. J., Jao, W.-C., & Dieterich, S. B. 2020, *AJ*, 160, 215
- Wang, J., Fischer, D. A., Xie, J.-W., & Ciardi, D. R. 2014, *ApJ*, 791, 111
- Waters, C., Magnier, E. A. & Pan-STARRS Science Consortium 2015, *IAUGA*, 29, 2256019
- Winters, J. G., Charbonneau, D., Henry, T. J., et al. 2021, *AJ*, 161, 63
- Winters, J. G., Henry, T. J., Lurie, J. C., et al. 2015, *AJ*, 149, 5
- Winters, J. G., Henry, T. J., Jao, W.-C., et al. 2019, *AJ*, 157, 216
- Zacharias, N., Finch, C. T., Girard, T. M., et al. 2012, VizieR Online Data Catalog
- Zacharias, N., Finch, C. T., Girard, T. M., et al. 2020, The Fourth U.S. Naval Observatory CCD Astrograph Catalog, IPAC, doi:10.26131/IRSA17
- Ziegler, C., Tokovinin, A., Briceño, C., et al. 2020, *AJ*, 159, 19